DOI: 10.23968/2500-0055-2022-7-1-23-32

RESEARCH ON MECHANICAL PROPERTIES AND GROUTABILITIES OF GROUTED MORTISE-TENON JOINTS FOR PREFABRICATED STRUCTURES

Huang Mingli[1], Shen Qiaofeng[2]*, Zhang Zhancheng[3]

[1]Beijing Jiaotong University
Haidian District, Beijing, 100044, China
[2]Emperor Alexander I St. Petersburg State Transport University
Moskovsky pr., 9, St. Petersburg, Russia
[3]China Overseas Engineering Group
Haidian District, Zizhuyuan Road No. 1, Beijing, China

*Corresponding author: 18813094515@163.com

Abstract
Introduction: The paper addresses grouted tenon-and-groove joints in the prefabricated structure of Changchun subway station. For the first time, grouting of prefabricated structure joints with organic epoxy grouting material is analyzed. **Purpose of the study:** We aimed to make sure that an organic epoxy grouting material can be injected into the joints uniformly and in full and conducted its experimental study. To establish the applicability of the epoxy grouting material in the prefabricated structures, we studied the mechanical properties of the epoxy grout and its adhesive properties in relation to concrete. **Methods:** In the course of the study, we used a set of test equipment and an independently developed method. **Results:** High-quality grouting can be guaranteed at an injection pressure of 0.4 MPa and a temperature of 5–10°C. The relationship between the slurry flow rate and time was fit according to the experimental data at 5 and 10°C. The optimal quartz powder ratio was determined at the level of 1:0.6–1:0.8, and the optimal quartz powder particle size (D50) was determined at the level of 18–25 μm. The results of the study can provide references for similar projects in the future.

Keywords
Prefabricated structure, grouted tenon-and-groove joints, epoxy grouting material, groutability, mechanical properties, experiment.

Introduction

Prefabrication is a construction technology that makes it possible to switch from traditional cast-in-situ concrete structures to prefabrication of components in a factory and on-site assembly. Due to its advantages, which include civilized construction, guaranteed construction quality, and reduced construction time, prefabrication will see broad application prospects in the coming decades with the rise of construction industrialization (Yan et al., 2004).

In China, Changchun Subway Line 2 encountered several problems: a tight construction schedule, high impact of construction on the surrounding environment, and low temperatures during the construction process. A number of open-cut subway stations were constructed using prefabrication and assembly technology. One of the stations has a single-arch, large-span structure assembled from seven prefabricated components with a ring width of 2 m. Fig. 1 shows a sectional diagram of the prefabricated structure. Fig. 2 shows ring and longitudinal connections between the members, made with a new type of grouted tenon-and-groove joint using concrete of grade C50 (Yang and Huang, 2018; Yang et al., 2019a).

Both domestic and foreign researchers have studied prefabricated assembled structures. Scandinavian countries and Russia have rich experience in the construction of prefabricated assembled subway stations (Li, 1995; Vlasov et al., 2002; Yurkevich, 1995). Li et al. (2019) analyzed the mechanical properties of two kinds of subway station structures (arched and rectangular) and concluded that the arched structure is characterized by better performance as well as lower stresses and deformations under the same load. Li and Liu (2016) analyzed factors affecting the bending stiffness of single tenon-and-groove joints in prefabricated subway stations and concluded that the bending moment of the joints is the most important factor leading to the reduction of their bending stiffness. An increase in the axial load and grouting of the joints significantly improves the bending stiffness of the

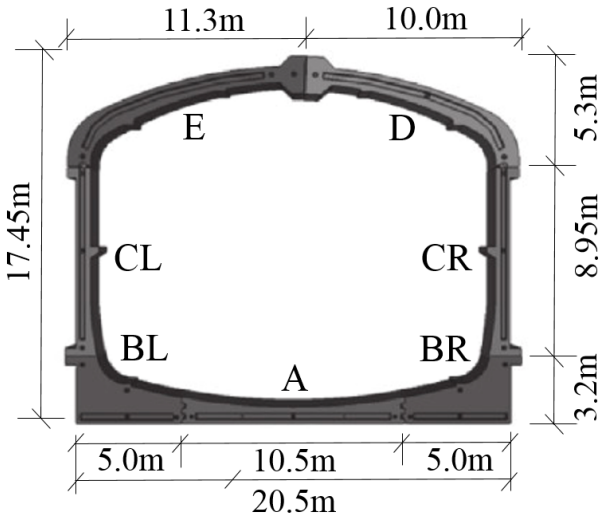

Fig. 1. Sectional diagram of the prefabricated structure

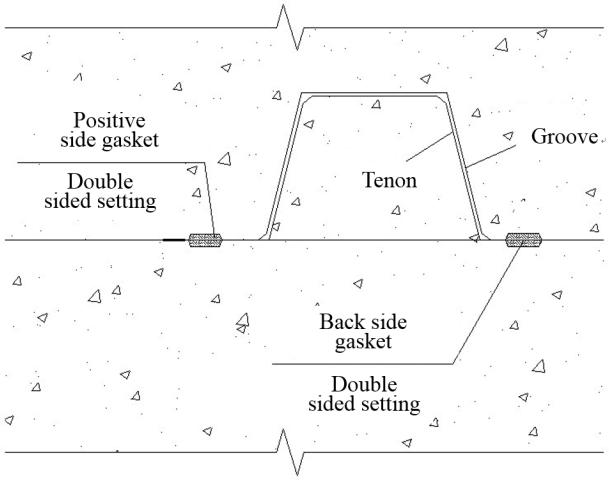

Fig. 2. Tenon-and-groove joints

joints. The degree of influence from changes in the dimensional parameters of the joint on its bending stiffness is related to the axial load applied to the joint. Su et al. (2016) conducted destructive tests on different combinations of axial and bending loads acting on different types of tenon-and-groove joints of fully assembled subway station structures to determine the flexural load-bearing capacity of the joints with account for five stages of flexural load bearing. Yang et al. (2019b, 2019c, 2020a, 2020b) performed a number of experiments to study the bending stiffness of grouted tenon-and-groove joints in prefabricated subway station structures and proposed a general formula for its calculation. Li et al. (2015a, 2015b, 2017, 2018) and Xu et al. (2017) systematically investigated the mechanical properties of tenon-and-groove joints in prefabricated structures using numerical simulations and structural loading tests, with the Yuanjiadian station of Changchun Metro Line 2 as the research background. Ding et al. (2018) and Tao et al. (2019) experimentally studied the seismic response characteristics of prefabricated subway station structures. Du et al. (2019) investigated the seismic performance of beam-slab-column joints in the cross-section of prefabricated assembled subway stations. Zhou et al. (2017) studied the tenon-and-groove grouting technology for prefabricated components.

Structural joints are still characterized by a design that is not very reliable. Bolted connections, pre-stressed rod connections, and cylindrical connections do not guarantee structural integrity. Water tightness cannot be guaranteed either. Although structural integrity and water tightness are guaranteed in weld and tenon-and-groove connections, the joined seams are filled with inorganic materials. The solidification and hardening of these materials are limited by temperature. Therefore, they are not suitable for use in low-temperature areas and low in adhesive strength (Wang et al., 2009).

Epoxy resin adhesives have a number of advantages. They are characterized by low shrinkage and strong adhesion to a variety of materials, easy to prepare and use. Besides, they ensure the high hardness of cured products and can be easily modified (Peng, 2004). To promote the further development of prefabricated assembled structures and solve issues with previous versions, epoxy resin was proposed as a potting material for joints. Inorganic rigid-particle quartz powder was used to modify it (Zhao and Yun, 1999). The influence of quartz powder introduction and the particle size on the mechanical properties of the epoxy grout and bonded concrete was studied experimentally. Researchers determined the optimal amount of quartz powder to be introduced and the particle size to develop the optimal epoxy grout formulation and conducted a full-scale test. To ensure successful grouting completion, Yang et al. (1997) studied epoxy grout injectability using unique test equipment and test methods that they developed, and analyzed the mechanical properties of the epoxy grout and bonded concrete.

Methods

1. Mechanical performance test model

The base fluid used for the test was epoxy resin with quartz powder particle sizes D50 of 16.71, 18.49, 21, 26.26, and 34.24 μm, and the test temperature was 13–14°C.

Compression strength and compression modulus were tested using GB 1041-79 plastic compression test method (State Standard of China, 1993). Shear bond strength was determined using three 100 × 100 mm C50 concrete test blocks bonded in triangles with epoxy grout as shown in Fig. 3. The test load was force-controlled with a loading rate of 0.2 KN/s. Tensile bond strength was determined by bonding two 100 × 100 mm C50 concrete specimens as shown in Fig. 4. The test load was displacement-controlled with a loading rate of 2 mm/min.

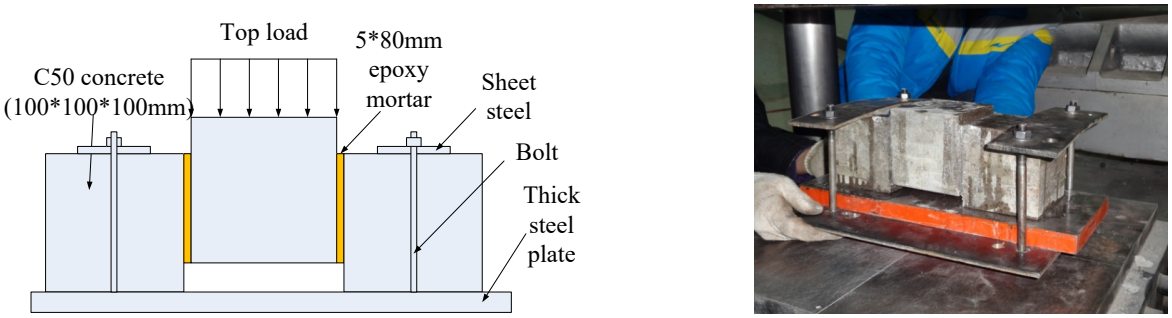

(a) Design drawing (b) Physical implementation

Fig. 3. Shear bond strength test system

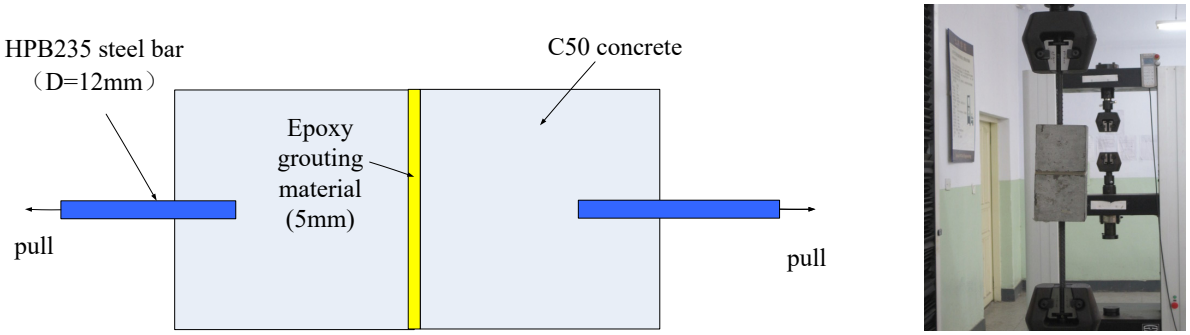

(a) Design drawing (b) Physical implementation

Fig. 4. Tensile bond strength test system

To study the load-bearing capacity of tenon-and-groove joints under different overburden loads, a full-scale test of tenon-and-groove joints was conducted. Due to the complex shape of the original structure, the test was simplified and the test specimen consisted of two rectangular reinforced concrete blocks with tenons and grooves, with 5 mm of epoxy grout in the middle of the tenon and groove. The concrete grade, reinforcement grade, and reinforcement rate of the specimens were the same as in the original structure. The test was performed by applying an axial load to one end of the specimen by a jack to simulate the overburden load, and the bending moment at the tenon and groove was applied by two forces of equal size at equal distance from the tenon and groove. The test load was force-controlled. Fig. 5 shows a schematic diagram of full-scale test loading.

2. Injectability test model

Due to the complex shape and large size of the original structure, the original structure was simplified for the test without changing the thickness of the joints. Fig. 6 shows an injection test device used in the test. Its cross-section is given in Fig. 7, and the longitudinal section is given in Fig. 8. The main design parameters of the injection test device were the following: the seam spacing was 100 mm (1/6 of the original structure), the seam thickness was 5 mm, the total length of the grouting section was 1.6 × 3 + 1.65 × 2 + 0.1 × 4 = 8.5 m, and the internal diameter of the grouting pipe was of the original structure.

The test system consisted of a grouting pump, grouting tank, injection test device, and slurry collecting bucket, with all components connected by a grouting pipe. Fig. 9 shows its design diagram, and Fig. 10 shows its physical implementation.

The test process was as follows:

(1) Connect the grouting pump, grouting tank, injection test device, and slurry collecting bucket with the grouting pipe, ensure firm and dense connection. Open the valve and ventilate to test the tightness of the test device.

(2) Calculate the required amount of slurry to be injected (mass = density x volume) and multiply by a factor of 1.2 to prevent the air from being injected into the test device and causing damage to it. Prepare slurry and take measures to maintain the slurry and chamber temperature at the test temperature, test viscosity at that temperature. Close the valve at the bottom of the grouting tank, open the tank, slowly pour in epoxy resin slurry, and then close the tank.

(3) Add a relatively small pressure to the air pump, open the valve at the bottom of the grouting tank, close the valve at the bottom of the grouting tank after slurry flows out from the grouting port, increase air pump pressure to the design value, then open the valve at the bottom of the grouting tank, and record the level of slurry with a marker every 5 s.

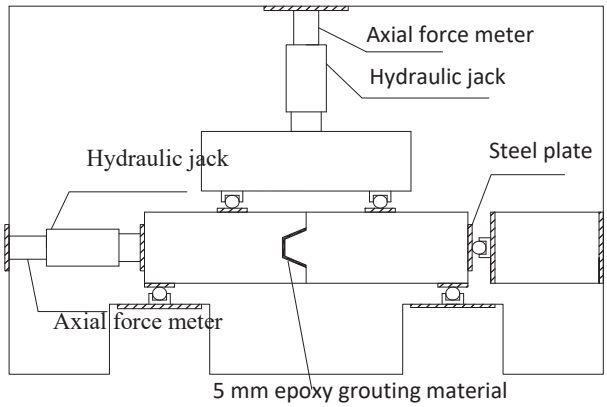

Fig. 5. Schematic diagram of full-scale test loading

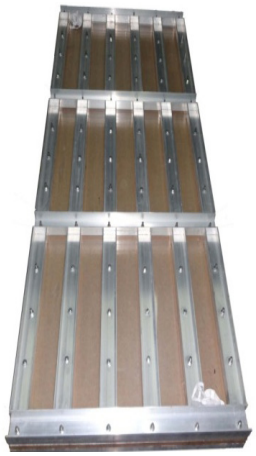

Fig. 6. Injection test device

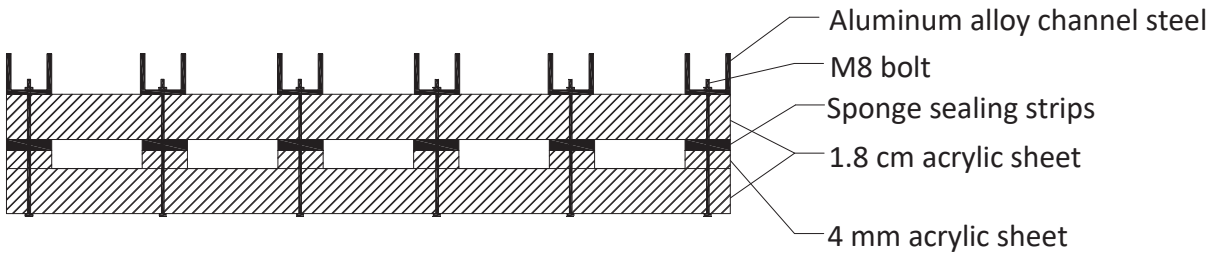

Fig. 7. Diagram of the cross-section

Fig. 8. Diagram of the longitudinal section

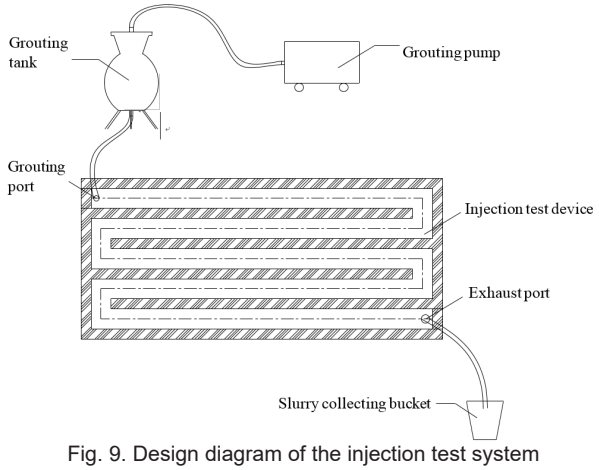

Fig. 9. Design diagram of the injection test system

Fig. 10. Injection test system

(4) After slurry injection, close the valve of the grouting tank and grouting pump.

Results

1. Mechanical performance test results

Fig. 11 shows the compressive strength of the epoxy grout vs. the amount of quartz powder, and Fig. 12 shows the elastic modulus of the epoxy grout vs. the amount of quartz powder.

Cao et al. (2005) studied the effect of adding ultrafine SiO_2 to epoxy resin on its mechanical properties and found that with small filler amounts, it is possible to reduce the shrinkage of epoxy resin,

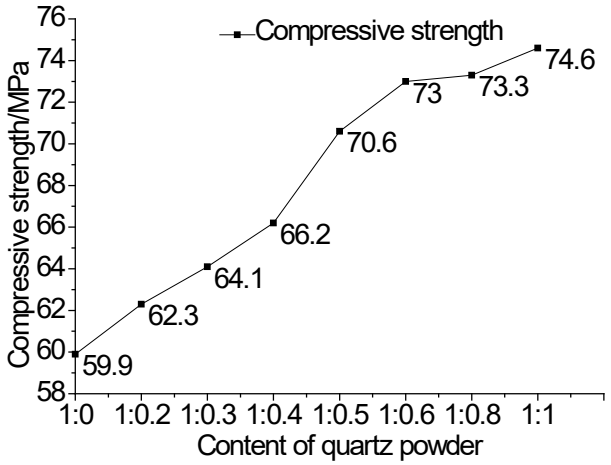

Fig. 11. Compressive strength of the epoxy grout vs. quartz powder amount

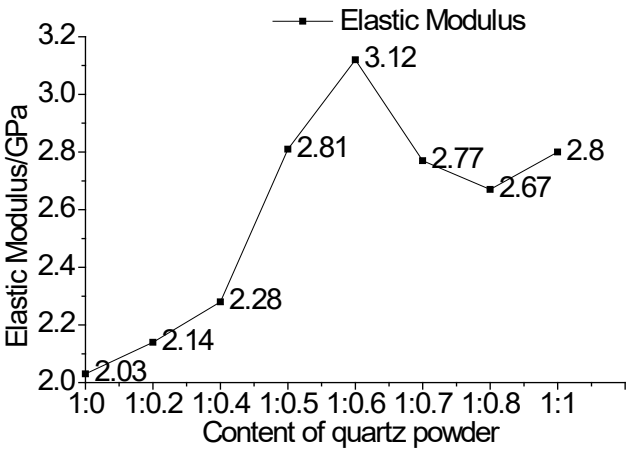

Fig. 12. Elastic modulus of the epoxy grout vs. quartz powder amount

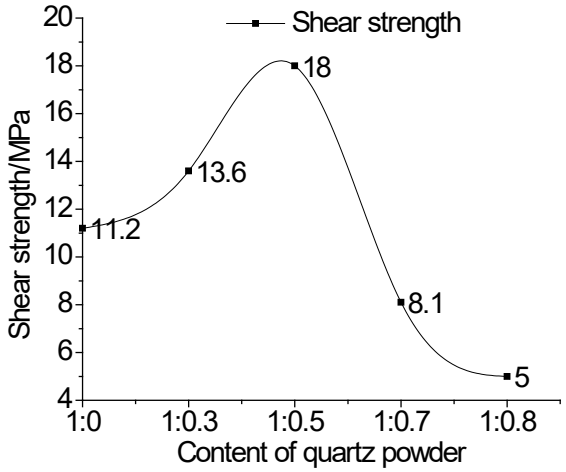

Fig. 13. Shear strength of epoxy grout bonded concrete vs. quartz powder amount

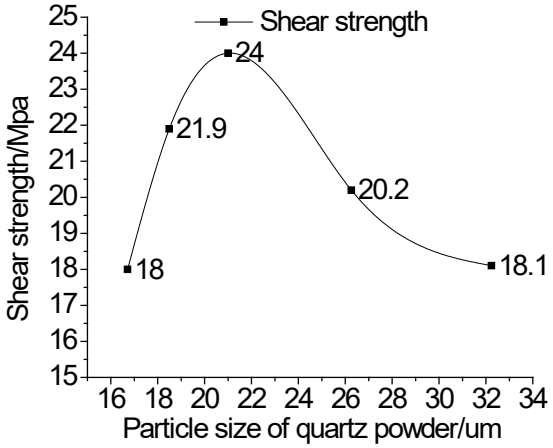

Fig. 14. Shear strength of epoxy grout bonded concrete vs. quartz powder particle size

absorb energy, and terminate the silver pattern, thus reducing residual stress during epoxy resin curing and uniforming the process. Therefore, with an increase in the filler ratio, the compressive strength will increase as well. However, when the filler amount exceeds a certain value, the stress fields generated by the filler overlap and dominate, and the compressive strength of epoxy resin decreases.

It can be seen from Fig. 11 that the compressive strength of epoxy mortar can exceed the compressive strength of C50 concrete. The compressive strength grows slowly when the quartz powder ratio is from 1:0.6 to 1:0.8 and is close to the maximum value.

As can be seen from Fig. 12, the elastic modulus of epoxy mortar first gradually increases with the addition of quartz powder, and then gradually decreases; it is close to the maximum value in the interval from 1:0.5 to 1:1. The introduction of quartz powder can improve the elastic modulus of epoxy resin since the elastic modulus of quartz powder is much larger than that of epoxy resin. Within a certain range of addition, quartz powder interacts better with the epoxy resin interface and resists the expansion of cracks, and beyond that range, the effect of quartz powder becomes smaller (You et al., 2006).

Fig. 13 shows the shear strength of epoxy grout bonded concrete vs. the amount of quartz powder. Fig. 14 shows the shear strength of epoxy grout bonded concrete vs. the size of quartz powder particles.

As can be seen from Fig. 13, with an increase in the amount of quartz powder when the ratio is less than 1:0.5, shear strength increases. It reaches the maximum value of 18 MPa when the ratio is 1:0.5, which is 60.7% higher than the shear strength of pure epoxy resin (11.2 MPa). When the ratio is greater than 1:0.5, shear strength gradually decreases. The reason is that when the amount of filler added is small, the filler particles do not interfere with each other and are uniformly dispersed in the epoxy resin matrix, and the filler makes it possible to reduce the shrinkage of the adhesive system, thus reducing residual stress during adhesive curing and uniforming the process. Therefore, with an increase in the

filler amount, the shear mechanical properties will improve. However, when the filler amount exceeds a certain value, the stress fields generated by the filler overlap, and the adhesive bonding performance and adhesive shear resistance decrease.

As can be seen from Fig. 14, with an increase in the quartz powder particle size (D50), the shear strength of epoxy grout bonded concrete first gradually increases and then gradually decreases, reaching a maximum value of 24 MPa when the quartz powder particle size (D50) is 21 μm. The reason is that when the quartz powder particle size (D50) increases but does not exceed 21 μm, the total area of quartz powder contact with concrete decreases after the epoxy grout is filled into the specimen, thus more epoxy resin can penetrate concrete and increase shear strength, while an increase in the area of epoxy resin contact with concrete will also increase shear strength. When the quartz powder particle size (D50) exceeds 21 μm, quartz powder deposition occurs during epoxy grout curing, thus, a part of the contact area between epoxy grout and concrete loses shear strength and the total shear strength decreases. Therefore, the quartz powder particle size (D50) shall be in the range from 18 to 25 μm, and this range can provide a better formulation.

The tensile strength of epoxy grout bonded concrete depending on the amount of quartz powder is shown in Table 1.

Table 1. Tensile strength (MPa)

Amount of quartz powder	Group 1	Group 2	Group 3	Group 4
1:0	2.53	2.88	2.96	2.79
1:0.5	2.52	2.79	2.84	2.72
1:0.8	2.66	2.73	2.81	2.73

The measurements and specimen damage diagram show that the tensile strength of the bonding surface of the epoxy grout bonded concrete specimens is much greater than the tensile strength of concrete. The specimens were damaged due to concrete failure. The value of tensile strength depends on the value of concrete tensile strength and has a weak relationship with the amount of quartz powder and particle size.

Fig. 15 shows the general damage pattern of full-scale test specimens. It can be seen that damage is distributed not along the tenon-and-groove joints but along the contact surface of reinforcement and concrete, and concrete on the joints peeled off at the time of damage, which indicates that the epoxy grout is safe for gluing tenon-and-groove joints.

To determine the flexural load-bearing capacity of the full-scale test specimens under different axial loads, three points of specimen damage were established: joint side opening of 3 mm when the corresponding bending moment is M_1; the end of the crack stable development stage when the corresponding bending moment is M_2; reinforcement stress reduction at the tenon-and-groove joint at the same time when the corresponding bending moment is M_3. In all three cases, the load-bearing capacity was taken as the smallest value among the bending moment values under the same axial load. The results are shown in Table 2.

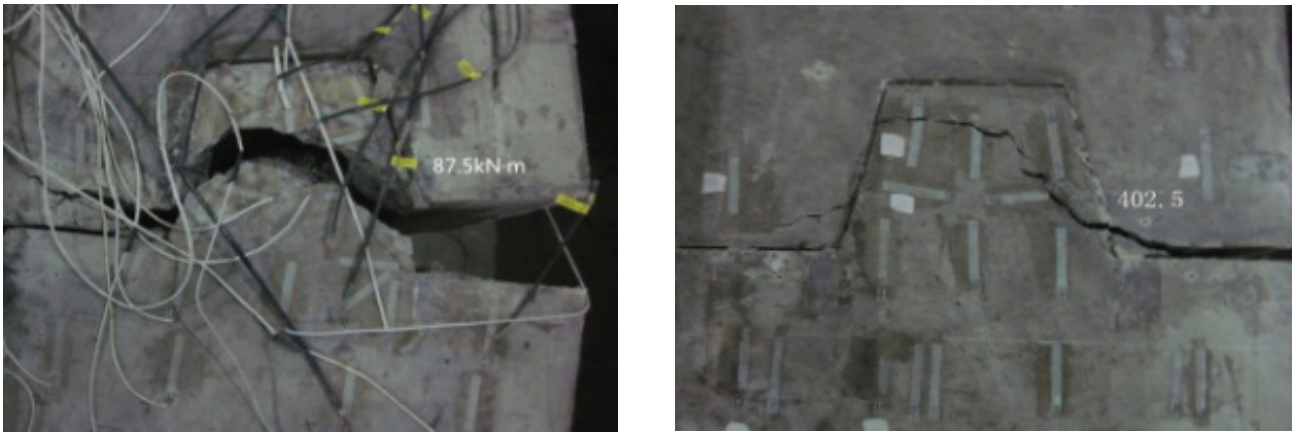

Fig. 15. Failure mode in the full-scale test

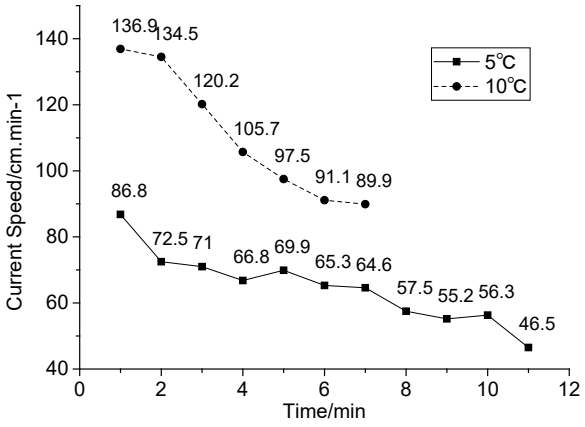

Fig. 16. Current speed vs. time

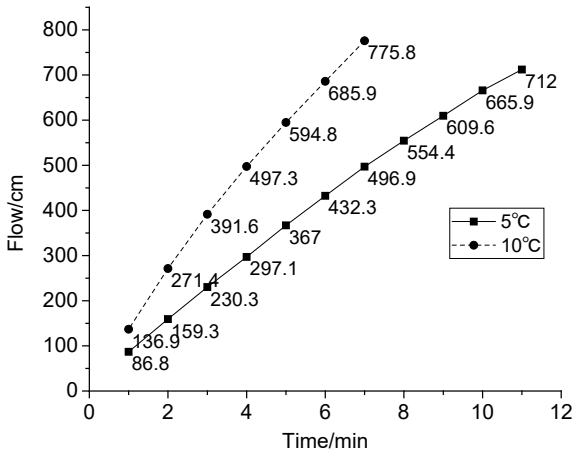

Fig. 17. Flow vs. time

Table 2. Flexural load-bearing capacity under different axial loads

Axial load	M_1	M_2	M_3	Load-bearing capacity
0	—	87.5	—	87.5
500	230	250	—	230
1000	335	326	330	326
1600	471	470	480	470
2000	593	500	550	500

2. Injectability test results

During the tests, we used a modified epoxy grout developed by Beijing Jiaotong University. The test pressure was 0.4 MPa. Fig. 16 shows a relationship between the flow rate and time, and Fig. 17 shows a relationship between the flow and time.

With an increase in the grouting distance, the flow rate gradually becomes slower, which is caused by the internal friction between the layers. In other words, viscosity plays an important role. To study the relationship between the grouting volume and time, the measured data were fit; the fitting results are shown in Fig. 18.

The fitting results show that the correlation between the fit curve and the measured data curve is as high as 0.999, indicating that the function obtained by fitting is in good agreement with the actual results. They also show that the slurry volume and time are approximately parabolic, and the relationship between the flow rate and time can be obtained by the derivation of the function of the flow rate vs. time:

- Flow rate vs. time at 5°C: V = –2.5822t + 78.556.
- Flow rate vs. time at 10°C: V = –9.1642t + 141.97.

The function shows that, with an increase in time, the flow rate decreases gradually. The flow rate at the beginning of grouting at 5°C is 78.556 cm/min, and it decreases at a rate of 2.5822 cm/min. The time of epoxy grout injection at 5°C is 30.4 min, and the longest injection distance is 12.02 m. The flow rate at the beginning of grouting at 10°Cis 141.97 cm/min, and it decreases at a rate of 9.1642 cm/min. According to these calculations, the time of epoxy grout injection at 10°C is 15.5 min, and the longest injection distance is 11.02 m. The theoretical time of grouting for the next joint at 5and 10°C calculated by the fitting formula is shown in Table 3.

Table 3. Theoretical time of joint grouting (min)

Joints		A	B	C	D, E
Grouting time	5°C	15.6	6.1	13.1	16.3
	10°C	9.2	3.5	7.6	9.6

The above test results do not consider the effect of concrete surface friction on injectability. To consider it, we performed two sets of comparative tests, one with the use of Plexiglas plates with grit 60 emery cloth on the inner surface and another without emery cloth. Fig. 19 shows a relationship between the flow rate and time.

Conclusion

(1) The results of the mechanical properties test for the epoxy grout and bonded concrete were obtained.

Considering the effect of quartz powder introduction on the compressive strength and elastic modulus of the epoxy grout as well as the effect on the shear strength of low-temperature epoxy grout bonded concrete and the project cost, while ensuring the best use of the tenon-and-groove joint, the optimal ratio of quartz powder was determined at the level of 1:0.6–1:0.8.

Considering the effect of the quartz powder particle size on the shear strength of low-temperature epoxy grout bonded concrete, the optimal quartz powder particle size (D50) was determined at the level of 18–25 μm.

The tensile strength of epoxy grout bonded concrete depends on the tensile strength of concrete and does not depend on the quartz powder amount and particle size in epoxy grout.

The full-scale test showed that it is possible to ensure that the mechanical properties of joints meet the engineering needs by bonding tenon-and-groove joints with epoxy grout.

(2) The results of the epoxy grout injectability test demonstrate the following:

With a construction temperature of 5°C or higher and a grouting pressure of 0.4 MPa, the grouting quality of all joints in the project can be guaranteed.

The flow rate decreases with grouting time, the epoxy grout injection time at 5°C is 30.4 min, and the longest injection distance is 12.02 m. The epoxy grout injection time at 10°C is 15.5 min, and the longest injection distance is 11.02 m. The relationship between the slurry flow rate and time was fit according to the experimental data at 5 and 10°C.

Friction has a relatively small effect on injectability.

The application of prefabricated structures in underground engineering has broad prospects. The design of joints is the key to the success or failure of prefabricated structures application. The results of the research on the grouting material ratio and grouting technical parameters in this paper can provide references for practical engineering.

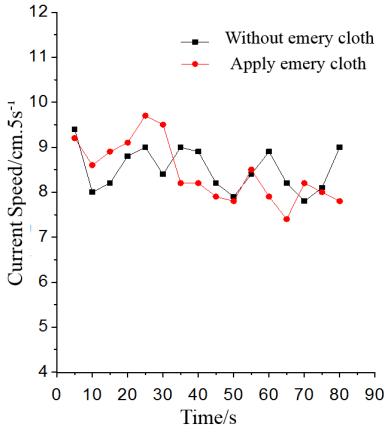

Fig. 18. Fitting results for the relationship between the flow and time

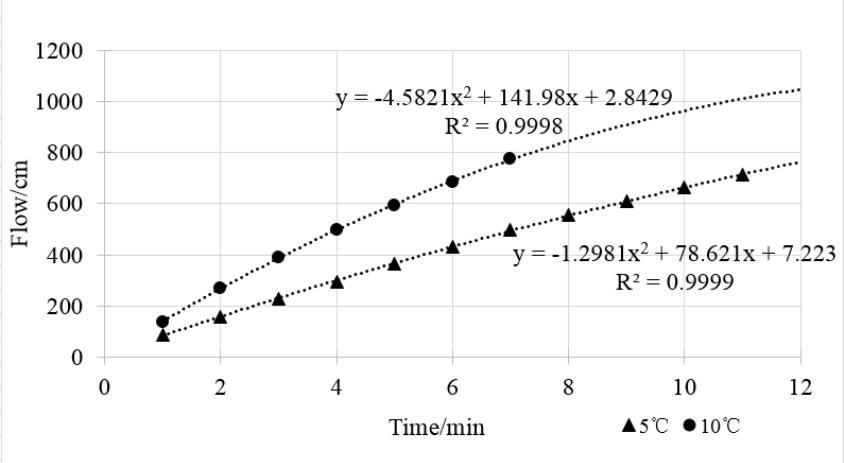

Fig. 19. Friction effect test diagram

References

Cao, P., You, M., Liu, G. and Cai, J. (2005). Effect of SiO2 on the strength of epoxy adhesives. *China Adhesives*, Vol. 14, Issue 4, pp. 15–17.

Ding, P., Tao, L., Yang, X., Zhao, J. and Shi, C. (2018). Three-dimensional dynamic response analysis of a single-ring structure in a prefabricated subway station. *Sustainable Cities and Society*, Vol. 45, pp. 271–286. DOI: 10.1016/j.scs.2018.11.010.

Du, X.-L., Liu, H.-T. and Xu, C.-S. (2019). Study on seismic performance of beam-column-slab interior joints in cross section of assembled monolithic subway station. *Journal of Building Structures*, Vol. 40, Issue 8, pp. 51–60.

Li, T.-H. (1995). Design and construction experience of Minsk single arch metro station. *Metro and Light Rail*, Vol. 2, pp. 44–48.

Li, Z.-P., Li, K.-X., L(u), S.-Q., Su, H.-F. and Wang, C. (2018). Experimental study on stress evolution rule of double tenon-groove joints for prefabricated metro station structure. *China Railway Science*, Vol. 39, Issue 5, pp. 15–21. DOI: 10.3969/j.issn.1001-4632.2018.05.03.

Li, X.-W. and Liu, Q. (2016). Influencing factor analysis of bending stiffness of single tenon groove joint of subway station constructed with prefabricated element. *Railway Standard Design*, Vol. 60, Issue 8, pp. 113–117. DOI: 10.13238/j.issn.1004-2954.2016.08.024.

Li, X.-H., Liu, C.-Y. and Zhang, Q. (2019). Comparative analysis of mechanical properties of arched and rectangular subway stations. *Construction Technology*, Vol. 48, Issue 16, pp. 1–4.

Li, Z.-P., Su, H.-F., Lu, S.-Q., Wang, C., and Xu, X.-Z. (2017). Experimental study on flexural mechanical properties of the double tenon groove joints of prefabricated subway station. *China Civil Engineering Journal*, Vol. 50, Issue S2, pp. 28–32.

Li, Z.-P., Wang, C., Su, H.-F., Shi, S.-F. (2015a). An experiment study on the evolution law of concrete structure crack and joint seam deformation for tenon groove joints in the prefabricated metro station. *China Civil Engineering Journal*, Vol. 48, Issue S1, pp. 409–413.

Li, Z.-P., Wang, C., Su, H.-F., Shi, S.-F. and Wang, P. (2015b). Mechanical property of tenon-groove joints for metro station constructed by prefabricated structure. *China Railway Science*, Vol. 36, Issue 5, pp. 7–11. DOI: 10.3969/j.issn.1001-4632.2015.05.02.

Peng, L.-G. (2004). *Study on epoxy resin adhesive for architecture structure*. Master's thesis. Xi'An: Xi'an University of Architecture and Technology.

State Standard of China (1993). GB/T 1041-92. *Test method for compressive properties of plastics*. Beijing: State Bureau of Quality and Technical Supervision.

Su, H.-F., Li, X.-W. and Wang, C. (2016). Experimental study on flexural capacity of joints of structure of metro station with prefabricated concrete structure. *Journal of the China Railway Society*, Vol. 38, Issue 9, pp. 118–123. DOI: 10.3969/j.issn.1001-8360.2016.09.017.

Tao, L., Ding, P., Shi, C., Wu, X., Wu, S. and Li, S. (2019). Shaking table test on seismic response characteristics of prefabricated subway station structure. *Tunnelling and Underground Space Technology*, Vol. 91, 102994. DOI: 10.1016/j.tust.2019.102994.

Vlasov, S. N., Alexandrov, V. N. and Kurakin, N. I. (2002). *Essentials of Russian underground railway construction*. Beijing: China Railway Press.

Wang, M.-N., Li, Z.-Y. and Wei, L.-H. (2009). *Prefabrication technology of tunnel and underground railway*. Chengdu: Southwest Jiaotong University Press.

Xu, X.-Z., Li, Z.-P., Zhu, Y.-C. and Su, H.-F. (2017). Study on shear property of tenon groove joint of prefabricated subway station. *China Civil Engineering Journal*, Vol. 50, Issue S2, pp. 141–146.

Yan, W., Cao, Y.-H. and Li, G.-R. (2004). Development of assembly-type RC structure and building industrialization. *Journal of Chongqing Jianzhu University*, Vol. 26, Issue 5, pp. 131–136.

Yang, X.-R. and Huang, M.-Q. (2018). Research strategies on new prefabricated technology of underground subway station. *Urban Rapid Rail Transit*, Vol. 31, Issue 1, pp. 78–85.

Yang, X.-R., Huang, M.-Q. and Lin, F. (2019a). Research strategies on new prefabricated technology for underground metro stations. *Urban Rail Transit*, Vol. 5, Issue 3, pp. 145–154. DOI: 10.1007/s40864-019-0106-z.

Yang, X.-R., Huang, M.-Q., Lin, F., Wang, C. and Su, H.-F. (2019b). Experimental method of grouted mortise-tenon joint for prefabricated metro station structure. *Urban Rapid Rail Transit*, Vol. 32, Issue 5, pp. 83–90.

Yang, X.-R., Huang, M.-Q. and Lin, F. (2020a). Research on bending resistance characteristics of grouted mortise-tenon joints for prefabricated metro station structures. China Civil Engineering Journal, Vol. 53, Issue 2, pp. 33–40.

Yang, X.-R., Lin, F. and Huang, M.-Q. (2020b). Experimental research on flexural rigidity of grouted single mortise-tenon joints for prefabricated metro station structures. *China Civil Engineering Journal*, Vol. 53, Issue 3, pp. 38–43.

Yang, X.-N., Lu, S.-L. and Ge, J.-L. (1997). Bolt-grouting support and its application in weak rock roadway. *Chinese Journal of Rock Mechanics and Engineering*, Vol. 16, Issue 2, pp. 171–177.

Yang, X.-R., Shi, Z.-H. and Lin, F. (2019c). Influence of geometrical parameters on performance of grouted mortise and tenon joints for application in prefabricated underground structures. *Advances in Civil Engineering*, Vol. 2019, 3747982. DOI: 10.1155/2019/3747982.

You, M., Cao, P., Wei, X.-H. and Yu, H.-Z. (2006). Effect of SiO2 filler on the elastic modulus and Poisson's ratio of epoxy layer. *China Adhesives*, Vol. 15, Issue 3, pp. 12–14.

Yurkevich, P. (1995). Developments in segmental concrete linings for subway tunnels in Belarus. *Tunnelling and Underground Space Technology*, Vol. 10, No. 3, pp. 353–365. DOI: 10.1016/0886-7798(95)00015-Q.

Zhao, S.-Q. and Yun, H.-M. (1999). Study on rigid particle toughened epoxy resin. *China Plastics*, Vol. 13, Issue 9, pp. 35–39.

Zhou, S., Zhang, X., Dong, J.-L., Li, S.-L. and Wang, Q.-B. (2017). Grouting technology of prefabricated groove for prefabricated metro station. *Building Technique Development*, Vol. 44, Issue 18, pp. 70–71.